



1           **Evaluation of high-resolution predictions of fine**  
2           **particulate matter and its composition in an urban area**  
3                                   **using PMCAMx-v2.0**  
4

5 Brian T. Dinkelacker<sup>1</sup>, Pablo Garcia Rivera<sup>1</sup>, Ioannis Kioutsioukis<sup>2</sup>, Peter J. Adams<sup>3,4</sup>,  
6 Spyros N. Pandis<sup>5,6</sup>

7  
8 <sup>1</sup>*Department of Chemical Engineering, Carnegie Mellon University, Pittsburgh, PA,*  
9 *15213*

10 <sup>2</sup>*Department of Physics, University of Patras, 26500, Patras, Greece*

11 <sup>3</sup>*Department of Civil and Environmental Engineering, Carnegie Mellon University,*  
12 *Pittsburgh, PA, 15213*

13 <sup>4</sup>*Department of Engineering and Public Policy, Carnegie Mellon University, Pittsburgh,*  
14 *PA, 15213*

15 <sup>5</sup>*Institute of Chemical Engineering Sciences (FORTH/ICE-HT), 26504, Patras, Greece*

16 <sup>6</sup>*Department of Chemical Engineering, University of Patras, 26500, Patras, Greece*

17 \*Correspondence to: Spyros N. Pandis (spyros@chemeng.upatras.gr)

18  
19 **Abstract**

20 Accurately predicting urban PM<sub>2.5</sub> concentrations and composition has proved challenging  
21 in the past, partially due to the resolution limitations of computationally intensive chemical  
22 transport models (CTMs). Increasing the resolution of PM<sub>2.5</sub> predictions is desired to  
23 support emissions control policy development and address issues related to environmental  
24 justice. A nested grid approach using the CTM PMCAMx-v2.0 was used to predict PM<sub>2.5</sub>  
25 at increasing resolutions of 36 x 36, 12 x 12, 4 x 4, and 1 x 1 km for a domain largely  
26 consisting of Allegheny County and the city of Pittsburgh in southwestern Pennsylvania,  
27 US during February and July 2017. Performance of the model in reproducing PM<sub>2.5</sub>  
28 concentrations and composition was evaluated at the finest scale using measurements from  
29 regulatory sites as well as a network of low-cost monitors. Total PM<sub>2.5</sub> mass is reproduced  
30 well by the model during the winter period with low fractional error (0.3) and fractional  
31 bias (+0.05) when compared to regulatory measurements. Comparison with speciated  
32 measurements during this period identified small underpredictions of PM<sub>2.5</sub> sulfate,  
33 elemental carbon (EC), and organic aerosol (OA) offset by a larger overprediction of PM<sub>2.5</sub>  
34 nitrate (bias = +1.4 μg m<sup>-3</sup>, fractional bias = +0.81). In the summer period, total PM<sub>2.5</sub> mass  
35 is underpredicted with fractional bias of -0.39. Here, PM<sub>2.5</sub> nitrate is overpredicted again  
36 with a large fractional bias (+0.7) but significantly lower magnitude (+0.4 μg m<sup>-3</sup>).



37 Underpredictions in PM<sub>2.5</sub> sulfate and EC contribute to the negative prediction bias of total  
38 PM<sub>2.5</sub> (-0.4 μg m<sup>-3</sup> and -0.2 μg m<sup>-3</sup>, respectively), however the largest underprediction is  
39 seen for summer OA (bias = -1.9 μg m<sup>-3</sup>, fractional bias = -0.41). In the winter period, the  
40 model performs well reproducing the variability between urban measurements and rural  
41 measurements of local pollutants such as EC and OA. This effect is also captured well in  
42 the summer for EC, although the OA performance here is less consistent because much  
43 more of this OA is secondary and transported from outside of the inner modeling domain.  
44 Comparison with total PM<sub>2.5</sub> concentration measurements from low-cost sensors yielded  
45 similar results with slightly higher overpredictions seen in the winter (fractional bias =  
46 +0.24) and lower underpredictions seen in the summer (fractional bias = -0.27).  
47 Inconsistencies in PM<sub>2.5</sub> nitrate predictions in both periods are believed to be due to errors  
48 in partitioning between PM<sub>2.5</sub> and PM<sub>10</sub> modes and motivate improvements to the treatment  
49 of dust particles within the model. The underprediction of summer OA would likely be  
50 improved by updates to biogenic SOA chemistry within the model, which would result in  
51 an increase of long-range transport SOA seen in the inner modeling domain. These  
52 improvements are obvious topics for future work towards model improvement.  
53 Comparison with regulatory monitors showed that increasing resolution from 36 km to 1  
54 km improved both fractional error and fractional bias by 0.04 in February 2017. In July  
55 2017, fractional error decreased by 0.05 and fractional bias improved by 0.07 with  
56 increasing resolution. Improvements at all types of measurement locations indicated an  
57 improved ability of the model to reproduce urban-rural PM<sub>2.5</sub> gradients at higher  
58 resolutions.

59

## 60 **1 Introduction**

61 Fine particulate matter with aerodynamic diameter less than 2.5 μm (PM<sub>2.5</sub>) has  
62 been associated with public health concerns due to short and long-term exposure. Some of  
63 the health effects of PM<sub>2.5</sub> include increased risk of heart disease, increased likelihood of  
64 heart attacks and strokes, impaired lung development, and increased risk of lung disease  
65 (Dockery and Pope, 1994). Chemical transport models are frequently used for supporting  
66 the development of air quality policies designed to protect public health. To evaluate these



67 policies, CTMs must simulate  $PM_{2.5}$  concentrations and their response to changes in  
68 emissions accurately.

69 Grid resolution is an important factor for CTM studies focusing on major urban  
70 areas since on-road traffic, commercial cooking, and biomass burning can have sharp  
71 gradients at the urban scale (Lanz et al., 2007; Allan et al., 2010). High spatial resolution  
72 measurements of  $PM_1$  in the city of Pittsburgh in high source-impact locations are on  
73 average 40% higher than at urban background locations (Gu et al., 2018). Heightened  
74 organic aerosol concentrations have been observed in commercial districts containing  
75 multiple restaurants (Robinson et al., 2018). The demographic characteristics of the  
76 population can also have large variations at the neighborhood scale. High resolution  
77 predictions of pollutant concentrations allow for exposure assessments that compare  
78 subpopulations within the same metropolitan area to answer environmental justice related  
79 questions (Anand, 2002). The benefits of high-resolution modeling must be balanced with  
80 the increased complexity in the development of accurate, high-resolution emission  
81 inventories and increased computational cost and storage requirements.

82 Previous studies have found small to modest improvements on the predictive ability  
83 of regional CTMs for ozone in the summers of 1995, 1996, and 1997 moving from 36 km  
84 to 12 km resolution (Arunachalam et al., 2006) as well as in July 1988 using a dynamic  
85 grid system with sizes varying from 18.5 km to 4.625 km (Kumar and Russell, 1996).  
86 Stroud et al. (2011) found that the accurate simulation of urban and large industrial plumes  
87 required a grid resolution of 2.5 km in order to properly capture contributions from local  
88 sources of primary organic aerosol (POA) and volatile organic compounds (VOCs).  
89 Zakoura and Pandis (2019) investigated the effect of increasing grid resolution on  $PM_{2.5}$   
90 nitrate predictions and found that increasing the resolution to 4 km reduced bias by 65%.  
91 Fountoukis et al. (2013) reported a reduction of the bias for black carbon (BC)  
92 concentrations in the northeastern US when the grid resolution was reduced from 36x36  
93 km to 4x4 km. Pan et al., (2017) allocated county-based emissions at 4 km and 1 km grid  
94 resolution using the default approach from the National Emissions Inventory and found  
95 small changes in model performance for  $NO_x$  and ozone. The 1 km simulation was able to  
96 resolve the detailed spatial variability of emissions in heavily polluted areas including  
97 highways, airports and industrially focused sub-regions.



98           One of the weaknesses of several of the above studies has been that the gridded  
99 emissions used at the higher resolutions were the results of interpolation. It is not clear if  
100 the remaining discrepancies between model predictions and measurements were due to  
101 errors in the spatial distribution of the high-resolution emissions, errors in the overall  
102 magnitude of the emissions over an urban area or other modeling errors in the simulation  
103 of various processes (chemistry, condensation/evaporation, etc.). It is also not clear if errors  
104 in previous simulations of urban  $PM_{2.5}$  are due to inaccuracies in the transport of regional  
105  $PM_{2.5}$  to urban areas. In this work, we explore the impacts of increasing the resolution of  
106 emissions inputs and CTM output on  $PM_{2.5}$  predictions in southwestern Pennsylvania  
107 during the months of February and July 2017, including the ability of the model to  
108 reproduce observed differences between urban and rural  $PM_{2.5}$  at the various grid  
109 resolutions.

110           Garcia Rivera et al. (2022) investigated the effects of increasing grid resolution of  
111 model inputs and CTM output on source resolved predictions of  $PM_{2.5}$  concentration and  
112 population exposure at 36 km, 12 km, 4 km, and 1 km. Moving to 12 x 12 km resolution  
113 resolved much of the urban-rural gradient. Increasing to 4 x 4 km resolved stationary  
114 sources such as power plants and the 1 x 1 km resolution results revealed intra-urban  
115 variations and individual roadways. Regional pollutants with low spatial variability such  
116 as  $PM_{2.5}$  nitrate showed modest changes when increasing the resolution to 4 x 4 km and  
117 higher. Local pollutants such as black carbon and organic aerosol showed gradients that  
118 were only resolved at the finest resolution. The ability of these simulations to reproduce  
119  $PM_{2.5}$  concentrations at different resolutions is evaluated here against multiple  
120 measurement sources and types.

121           We apply the Particulate Matter Comprehensive Air quality Model with Extensions  
122 version 2.0 (PMCAMx-v2.0) to study the impact of increasing model resolution on the  
123 ability to reproduce observed  $PM_{2.5}$  concentrations. We evaluate the PMCAMx predictions  
124 at various grid resolutions against regulatory measurements of  $PM_{2.5}$  concentration and  
125 composition, as well as measurements from a network of low-cost sensors (Zimmerman et  
126 al., 2018) during February and July 2017 which provide a unique opportunity for  
127 comparison not available to previous studies. Aerosol mass spectrometer (AMS)



128 measurements taken in Pittsburgh during February 2017 were also used to evaluate model  
129 predictions.

130

## 131 **2 Model Description**

132 PMCAMx-v2.0, the Particulate Matter Comprehensive Air Quality Model with  
133 Extensions (Karydis et al., 2010; Murphy and Pandis, 2010; Tsimpidi et al., 2010) is a  
134 state-of-the-art atmospheric chemical transport model (CTM) that uses the framework of  
135 the CAMx model (Environ, 2006) with advanced aerosol chemistry modules. To track the  
136 dynamic evolution of aerosol mass, 10 moving size sections are used (Gaydos et al., 2003).  
137 The chemical mechanism SAPRC99 (Carter, 1999) was used for gas-phase chemistry,  
138 including 237 individual chemical reactions involving 91 chemical species. Aqueous-phase  
139 chemistry is calculated with the Variable Size Resolution Model (Fahey and Pandis, 2001).  
140 PMCAMx-v2.0 considers the formation of aerosol mass comprised of sulfate, nitrate,  
141 ammonium, sodium, chloride, water, elemental carbon, as well as lumped organic species  
142 (both primary and secondary). Inorganic aerosol growth is modelled using an approach that  
143 assumes equilibrium between the bulk aerosol and gas phases. Partitioning of semivolatile  
144 inorganic aerosol is calculated using ISORROPIA-I (Nenes et al., 1998). The Volatility  
145 Basis Set (VBS) was used to calculate partitioning of organic aerosol components across a  
146 distribution of species volatility (Donahue et al., 2006). Volatility bins (10) with effective  
147 saturation concentration from  $10^{-3}$  to  $10^6 \mu\text{g m}^{-3}$  (at 298 K) are used for primary organic  
148 aerosol (POA). Secondary organic aerosol is split into anthropogenic (aSOA) and biogenic  
149 (bSOA) components, formed from a variety of SOA-forming volatile organic compounds  
150 (VOCs) from human activity and natural sources, respectively using  $\text{NO}_x$ -dependent SOA  
151 formation yields (Lane et al., 2008). Both aSOA and bSOA are split into 4 volatility bins  
152 with effective saturation concentration from  $10^0$  to  $10^3 \mu\text{g m}^{-3}$  (at 298 K).

153

## 154 **3 Model Application**

155 Air quality simulations of a 5184 km<sup>2</sup> area comprised of southwestern Pennsylvania  
156 and smaller parts of eastern Ohio and northern West Virginia were performed using  
157 PMCAMx. Two distinct simulation periods of February and July 2017 were investigated.  
158 The approach of Garcia et al. (2022) was used to produce speciated  $\text{PM}_{2.5}$  concentration



159 predictions at spatial resolution of 36 km, 12 km, 4 km, and 1 km. Surface-level boundary  
160 conditions for the 36 x 36 km simulations are provided in Table S1. Boundary conditions  
161 for the higher resolution grids are taken from the results of parent-grid simulations. The  
162 first two days of simulation output have been removed from the analysis to allow for model  
163 spin-up.

164 Meteorological fields were calculated using the Weather Research and Forecasting  
165 model (WRF-v3.6.1) with horizontal resolution of 12 x 12 km, providing wind  
166 components, eddy diffusivity, temperature, pressure, humidity, clouds, and precipitation  
167 inputs for use in PMCAMx. Meteorology initial and boundary conditions were retrieved  
168 from the ERA-Interim global climate re-analysis database. The United States Geological  
169 Survey database was used to obtain input data for terrain, land-use, and soil type. When  
170 necessary, WRF output was interpolated to higher resolutions. An evaluation of  
171 interpolated meteorological inputs using data from METAR stations near the city of  
172 Pittsburgh in southwestern Pennsylvania determined that errors in the magnitude and  
173 phasing of diurnal cycles of temperature, relative humidity, and wind speed are  
174 appropriately small for use in air quality studies. These results are provided in the  
175 supplementary material (Fig. S1, S2).

176 Anthropogenic emissions are derived from the 2017 projections of the 2011  
177 National Emissions Inventory (Eyth and Vukovich, 2016) modelling platform. The Sparse  
178 Matrix Operator Kernel Emissions modeling system (SMOKE) was used, along with  
179 meteorological inputs to calculate emissions at a horizontal resolution of 12 x 12 km.  
180 Default spatial surrogates were used to allocate these emissions to higher resolutions.  
181 Custom surrogates were developed for commercial cooking and on-road traffic emissions  
182 sectors and used for the primary analysis in this work.

183 For commercial cooking, the normalized restaurant count was used to distribute the  
184 emissions from the sector in space within the 1 x 1 km and 4 x 4 km domains. This surrogate  
185 distributed commercial cooking emissions based on the density of restaurants identified by  
186 the Google Places Application Programming Interface. To allocate on-road traffic  
187 emissions, the output from the traffic model of Ma et al. (2020) was used. This model  
188 simulates hourly traffic using data from the Pennsylvania Department of Transportation.  
189 Emissions from the on-road traffic sector were then allocated based on these values.



190

### 191 **3.1 Available measurements for model evaluation**

192 Model predictions of sulfate, nitrate, elemental carbon and organic aerosol were  
193 compared with measurements from 4 sites from the EPA Chemical Speciation Network  
194 (EPA-CSN) (U.S. EPA, 2002). The locations of these 4 sites are shown in Figure 1a. These  
195 sites include: Lawrenceville, an urban background site 4 km northeast of downtown  
196 Pittsburgh; Hillman State Park located in a state park in southwest Pennsylvania in a rural  
197 and remote location approximately 40 km upwind of Pittsburgh; Steubenville in the Ohio  
198 River Valley close to industrial installations and coal-fired power plants, and the Liberty-  
199 Clairton monitor, which is located close to the Clairton Coke Works in the Monongahela  
200 River Valley 14 km southeast of downtown Pittsburgh. Speciated PM<sub>2.5</sub> measurements  
201 from EPA-CSN sites are available every three days during the simulation periods. Daily  
202 non-speciated measurements of total PM<sub>2.5</sub> mass concentration are available from 17 sites  
203 within the inner simulation domain and are used to further evaluate total PM<sub>2.5</sub> mass  
204 concentration predictions. The locations of these sites are also shown in Figure 1a.

205 For February 2017, high-resolution AMS measurements from the Carnegie Mellon  
206 University supersite (Gu et al., 2018) are used to evaluate the predicted chemical  
207 composition of PM<sub>2.5</sub> model predictions. Positive matrix factorization results are also used  
208 to investigate the breakdown of organic aerosol components. AMS measurements were  
209 taken continuously from February 1 to February 14, 2017. Due to uncertainties with the  
210 AMS collection efficiency during this campaign, we use here only the fractional particle  
211 composition data.

212 PMCAMx predictions of PM<sub>2.5</sub> were also compared with measurements taken with  
213 a network of Real-time Affordable Multi-Pollutant (RAMP) monitors (Zimmerman et al.,  
214 2018) distributed in the city of Pittsburgh. During the winter period measurements at 7 sites  
215 were available, all located within the boundaries of the city of Pittsburgh, while 22 sites  
216 were in operation during the summer period with a few sites also outside the city (Fig. 1b).  
217 Uncertainty in these low-cost measurements of PM<sub>2.5</sub> mass concentration is between 3-4  
218  $\mu\text{g m}^{-3}$  for hourly averaging times (Malings et al., 2019).

219 The model performance is assessed in terms of the mean bias (BIAS), the mean  
220 error (ERROR), the fractional bias (FBIAS) and the fractional error (ERROR):



$$221 \quad \text{BIAS} = \frac{1}{N} \sum_{i=1}^N P_i - O_i \quad (1)$$

$$222 \quad \text{FBIAS} = \frac{2}{N} \sum_{i=1}^N \frac{P_i - O_i}{P_i + O_i} \quad (2)$$

$$223 \quad \text{ERROR} = \frac{1}{N} \sum_{i=1}^N |P_i - O_i| \quad (3)$$

$$225 \quad \text{FERROR} = \frac{2}{N} \sum_{i=1}^N \frac{|P_i - O_i|}{P_i + O_i} \quad (4)$$

224

226 where  $N$  is the number of valid measurements,  $P_i$  is the predicted concentration and  $O_i$  is  
227 the corresponding observed concentration. The fractional error metric is bounded by 0  
228 (perfect prediction performance) and 2.0 (extremely poor prediction performance).  
229 Fractional bias is bounded by -2.0 (extreme underprediction) and +2.0 (extreme  
230 overprediction).

231

## 232 **4 Evaluation of high-resolution model performance**

### 233 **4.1 Winter**

234 Table 1 summarizes the performance metrics of daily average PMCAMx-v2.0  
235 PM<sub>2.5</sub> predictions in the 1x1 km resolution, when compared with daily measurements from  
236 EPA regulatory PM<sub>2.5</sub> monitors. The speciated performance is illustrated in Figure 2.  
237 Predictions of total PM<sub>2.5</sub> mass perform well against regulatory measurements in the  
238 February simulation period, with fractional error of 0.3 and fractional bias of +0.07.

239 Average measured PM<sub>2.5</sub> sulfate for this time period was 1.9 μg m<sup>-3</sup>. Lower sulfate  
240 levels were observed at the Lawrenceville site in Pittsburgh (1.2 μg m<sup>-3</sup>) while significantly  
241 higher levels were observed at the Steubenville site (3.1 μg m<sup>-3</sup>). Predicted domain-average  
242 PM<sub>2.5</sub> sulfate at 1 x 1 km resolution was 1.3 μg m<sup>-3</sup>. Overall fractional error for sulfate  
243 predictions was 0.41 and no overall bias was observed (fractional bias of -0.02). PM<sub>2.5</sub>  
244 sulfate was slightly overpredicted at Hillman State Park (+0.18 fractional bias) and  
245 Lawrenceville (+0.25 fractional bias) and underpredicted at the industrial sites,  
246 Steubenville (-0.24 fractional bias) and Liberty/Clairton (-0.43 fractional bias) where  
247 observed PM<sub>2.5</sub> sulfate concentrations were higher.





248 Overpredictions were seen for PM<sub>2.5</sub> nitrate, with a fractional bias of +0.81. The  
249 average measured concentration at EPA-CSN sites within the simulation domain was 1.5  
250  $\mu\text{g m}^{-3}$ , while the domain-average predicted concentration was 1.8  $\mu\text{g m}^{-3}$ . Observed  
251 average PM<sub>2.5</sub> nitrate concentrations at Hillman State Park and Lawrenceville were slightly  
252 lower at 1.1  $\mu\text{g m}^{-3}$  and 1.2  $\mu\text{g m}^{-3}$ , respectively. Nitrate at the Steubenville location was  
253 observed to be higher on average at 2.2  $\mu\text{g m}^{-3}$ . This overprediction is seen at all sites but  
254 is particularly prevalent at Hillman State Park, Lawrenceville, and Liberty/Clairton, where  
255 errors are of the order of a factor of two. Previous PMCAMx modeling studies have found  
256 similar over-predictions. Part of this overprediction was due to the use of coarse-grid  
257 resolution (Zakoura and Pandis, 2018), but this is unlikely to be the cause here, because  
258 81% of the predicted domain-average nitrate is transported from outside of the inner  
259 modeling domain. These inconsistencies in PM<sub>2.5</sub> nitrate predictions are likely due to errors  
260 in the partitioning of nitrate between the fine (PM<sub>2.5</sub>) and coarse (PM<sub>10</sub>) modes, resulting  
261 in an overprediction of PM<sub>2.5</sub> nitrate. Resolving this modeling error likely requires  
262 improvements to the treatment of dust within the model, and the use of a dynamic approach  
263 for inorganic aerosol calculations rather than the bulk equilibrium approach.

264 The behavior of PM<sub>2.5</sub> ammonium measurements is similar to that of nitrate as most  
265 of it is in the form of ammonium nitrate. The average measured concentration at the four  
266 EPA-CSN stations was 0.9  $\mu\text{g m}^{-3}$ . At Hillman State Park and Lawrenceville, the measured  
267 average was lower at 0.5  $\mu\text{g m}^{-3}$  but higher at the Liberty/Clairton location at 2.1  $\mu\text{g m}^{-3}$ .  
268 PM<sub>2.5</sub> ammonium was overpredicted similarly to PM<sub>2.5</sub> nitrate with +0.83 fractional bias.  
269 The average measured concentration of PM<sub>2.5</sub> elemental carbon at EPA-CSN sites during  
270 February 2017 was 1.1  $\mu\text{g m}^{-3}$ . Elemental carbon concentrations are more localized than  
271 the inorganic PM<sub>2.5</sub> components. At Hillman State Park the average measured  
272 concentration was only 0.5  $\mu\text{g m}^{-3}$  while at Liberty/Clairton the averaged measured  
273 concentration was 2.9  $\mu\text{g m}^{-3}$ . For elemental carbon, the predicted domain-average was 0.4  
274  $\mu\text{g m}^{-3}$ . Average elemental carbon concentration in the 4 x 4 km simulation grid outside of  
275 the inner modeling domain was 0.3  $\mu\text{g m}^{-3}$ . Black carbon predictions at all sites had a  
276 fractional error of 0.71 with fractional bias of -0.08. Elemental carbon was overpredicted  
277 at the urban site with fractional bias of 0.73 and underpredicted at the other sites.



278 Average measured OA during this period was  $4.4 \mu\text{g m}^{-3}$ , but with significant  
279 spatial variability. At Hillman State Park and Lawrenceville measured OA was  $3.1 \mu\text{g m}^{-3}$   
280 and  $3.4 \mu\text{g m}^{-3}$ , respectively. At Liberty/Clairton and Steubenville the average measured  
281 OA was  $7 \mu\text{g m}^{-3}$  and  $6.3 \mu\text{g m}^{-3}$ , respectively. Domain-average predicted OA was  $2.2 \mu\text{g}$   
282  $\text{m}^{-3}$ . Outside of the inner  $1 \times 1 \text{ km}$  domain, average predicted OA was  $1.6 \mu\text{g m}^{-3}$ ,  
283 suggesting that the majority of predicted OA is transported from outside of the  $1 \times 1 \text{ km}$   
284 grid. Overall OA prediction performance in the winter is acceptable at 0.53 fractional error  
285 and low fractional bias (-0.01). At individual sites, performance varies. OA is predicted  
286 with low fractional bias (-0.10) at the rural Hillman State Park site. OA is overpredicted by  
287 with +0.31 fractional bias at the urban site in Lawrenceville and underpredicted at both  
288 industrial sites. An added degree of uncertainty exists with the industrial sites within the  
289 inner domain. The emissions from these sources may be underestimated in the inventory  
290 and these locations are also difficult to accurately model due to their geographic location  
291 in river valleys.

292 Average concentrations of  $\text{PM}_{2.5}$  sulfate, nitrate, and ammonium in the  $4 \times 4 \text{ km}$   
293 resolution domain were around 83% of the average predicted concentrations in the inner  $1$   
294  $\times 1 \text{ km}$  simulation grid. For elemental carbon and OA, the outer concentration was 64%  
295 and 73% of the inner concentration respectively, indicating that these species had  
296 significant local sources. For these more local pollutants, the model appears to perform  
297 well in terms of capturing urban-rural gradients, but with a tendency towards  
298 underprediction at the rural site in Hillman State Park and overprediction at the urban site  
299 in Lawrenceville. The model also underpredicts EC and OA at the industrial locations,  
300 especially elemental carbon (-0.67 and -1.02 fractional bias at Steubenville and  
301 Liberty/Clairton, respectively). This again suggests errors in the emissions inventory or  
302 problems in simulating atmospheric dispersion near the sources.

303 Comparisons with the  $\text{PM}_1$  composition as determined by the AMS from February  
304 3 through February 14, 2017, show excellent agreement for all species (Fig. 3a). Gu et al.  
305 (2018) used PMF analysis and allocated total measured OA into five factors. Three of them  
306 corresponded to primary organic aerosol: hydrocarbon-like OA (HOA), cooking OA  
307 (COA) and biomass burning OA (BBOA) and two secondary OA factors: more-oxidized  
308 organic aerosol (MO-OOA) and less-oxidized organic aerosol (LO-OOA). To compare



309 PMCAMx predictions with the primary PMF factors, two additional simulations were  
310 performed in which emissions from biomass burning and commercial cooking were set to  
311 zero. The predicted concentrations were then subtracted from the base case to estimate the  
312 contribution from each respective source. The remaining primary OA was assigned to  
313 HOA. The LO-OOA and MO-OOA factors were added together and compared with the  
314 PMCAMx SOA predictions.

315 The predicted cooking OA (COA) at the CMU site is 25% of the total OA and is in  
316 agreement with the PMF/AMS estimate of 22% (Fig. 3b). This is encouraging given the  
317 small bias of the model for total OA levels. The predicted HOA and BBOA are higher than  
318 measured by a factor of 2 or more. At the same time, the measurements indicate a  
319 surprisingly high contribution of SOA (53% of the total OA) during a period with little  
320 photochemical activity and low levels of OH radicals. SOA is predicted to be just 20% of  
321 the total during this time period. These discrepancies may indicate transformation of the  
322 HOA and BBOA to OOA during this wintertime period, that are not included in the model.  
323 Kodros et al. (2021) recently suggested that BBOA can react with the  $\text{NO}_3$  during the  
324 winter and can be transformed to OOA.

325

#### 326 **4.2 Summer**

327 Total  $\text{PM}_{2.5}$  mass concentrations are underpredicted in the summer period. The  
328 average measured  $\text{PM}_{2.5}$  value in the regulatory network in the area was  $11.4 \mu\text{g m}^{-3}$ , while  
329 the average predicted value at the regulatory sites was  $4 \mu\text{g m}^{-3}$  lower.

330 Speciated  $\text{PM}_{2.5}$  performance is illustrated in Figure 4. Average measured  $\text{PM}_{2.5}$   
331 sulfate for the summer period was  $2 \mu\text{g m}^{-3}$ . Slightly lower levels were observed at the  
332 Lawrenceville site in Pittsburgh ( $1.9 \mu\text{g m}^{-3}$ ). Liberty/Clairton had higher measured sulfate  
333 concentrations ( $2.6 \mu\text{g m}^{-3}$ ), but this difference between locations is lower than what was  
334 observed in the winter period. Predicted domain-average  $\text{PM}_{2.5}$  sulfate at  $1 \times 1 \text{ km}$   
335 resolution was  $1.3 \mu\text{g m}^{-3}$ . Overall fractional error (0.62) and fractional bias (-0.21) for  
336 sulfate predictions was higher than in the winter simulation period.  $\text{PM}_{2.5}$  sulfate was  
337 underpredicted at all sites but to the largest extent at Hillman State Park (-0.36 fractional  
338 error).



339 Overpredictions of PM<sub>2.5</sub> nitrate were also seen the summer period, and at all types  
340 of sites. Average measured PM<sub>2.5</sub> nitrate was 0.3 μg m<sup>-3</sup>, much lower than in the winter.  
341 The domain-average predicted PM<sub>2.5</sub> nitrate was 0.7 μg m<sup>-3</sup>. Again, predicted PM<sub>2.5</sub> nitrate  
342 in the inner domain is dominated by material transported from outside the boundaries  
343 (75%), so the issue is not resolved by using a high-resolution grid. Improvements to PM<sub>2.5</sub>  
344 nitrate formation are needed in the form of dust models with increased complexity to  
345 resolve the issues with fine-coarse mode partitioning of particulate nitrate. These issues  
346 have been highlighted by decreased concentrations of PM<sub>2.5</sub> pollution in recent years.

347 Observed PM<sub>2.5</sub> ammonium concentrations at EPA-CSN sites were also much  
348 lower in the summer with an average value of 0.5 μg m<sup>-3</sup>. Slightly higher average  
349 concentrations were observed at Liberty/Clairton (0.7 μg m<sup>-3</sup>) and slightly lower  
350 concentrations were observed at Steubenville (0.4 μg m<sup>-3</sup>). The domain-average predicted  
351 PM<sub>2.5</sub> ammonium concentration was 0.6 μg m<sup>-3</sup>. The average concentration directly outside  
352 of the inner domain was 0.5 μg m<sup>-3</sup>. Overall performance was better for ammonium in the  
353 summer than in the winter with fractional error of 0.62 and fractional bias of +0.44. The  
354 strongest overprediction is seen at the Steubenville site (+0.57 fractional bias).

355 The average measured elemental carbon (EC) concentration in July was 0.7 μg m<sup>-3</sup>  
356 <sup>3</sup>. Measured EC carbon was significantly higher at Liberty/Clairton (1 μg m<sup>-3</sup>) and lower  
357 at rural Hillman State Park (0.4 μg m<sup>-3</sup>). Domain-average predicted EC was 0.3 μg m<sup>-3</sup>.  
358 Outside of the inner domain, the average predicted concentration was 0.2 μg m<sup>-3</sup>. Elemental  
359 carbon predictions in July had a lower fractional error compared to the winter at 0.60 but  
360 showed a stronger negative fractional bias at -0.33. The model severely underpredicts at  
361 Hillman State Park (-0.86 fractional bias), where measured concentrations were lowest, but  
362 also at the industrial sites of Steubenville (-0.55 fractional bias) and Liberty/Clairton (-0.65  
363 fractional bias). EC was slightly overpredicted at the urban Lawrenceville location (+0.14  
364 fractional bias). While the urban-rural gradient in EC is slightly overpredicted, the model  
365 is still able to capture well the variability between rural (Hillman State Park) and urban  
366 (Lawrenceville). The model struggles to reproduce high measurements of EC at the  
367 Steubenville site, reiterating the issues with industrial EC seen in the winter.

368 Average measured OA concentration was 4.5 μg m<sup>-3</sup> in July. Higher concentrations  
369 were observed at the industrial sites, Liberty/Clairton and Steubenville (5.0 μg m<sup>-3</sup>)



370 respectively. The lowest observed concentration was in Hillman State Park ( $3.6 \mu\text{g m}^{-3}$ ).  
371 The average predicted concentration at CSN sites was  $2.7 \mu\text{g m}^{-3}$ . On average, OA is  
372 underpredicted with fractional bias of -0.47. This underprediction occurs at all sites but is  
373 less prevalent at the urban Lawrenceville location (-0.19 fractional bias) and is most  
374 dramatic in Steubenville (-0.65 fractional bias). Because such a large fraction of the OA in  
375 the summer is predicted to be secondary (50% of local OA on average) and transported  
376 from outside of the inner modeling domain (84% of total OA), treatment of SOA formation  
377 is likely a key factor contributing to the underprediction of  $\text{PM}_{2.5}$  in the summer. While  
378 these improvements are necessary for overall model improvement, they do not have  
379 significant impact on the urban-rural gradients which are the focus of this work and are  
380 driven by primary species. The performance of EC predictions in various locations is  
381 encouraging with regards to primary  $\text{PM}_{2.5}$  performance.

382

### 383 **5 Effect of grid resolution on $\text{PM}_{2.5}$ performance**

384 To determine the effect of grid resolution on the ability of the model to resolve  
385 geographical variations in  $\text{PM}_{2.5}$  concentrations, daily average measurements from the 17  
386 EPA regulatory sites were compared with PMCAMx predictions from simulations at 36  
387 km, 12 km, 4 km and 1 km. The PMCAMx performance metrics are summarized in Table  
388 2.

389

#### 390 **5.1 Winter**

391 During the winter period, increasing grid resolution reduces the average fractional  
392 error from 34% at 36 x 36 km to 30% at 1 x 1 km. The higher resolution also improved the  
393 fractional bias, from -0.09 at 36 x 36 km to +0.05 at 1 x 1 km. The performance is illustrated  
394 in Figure 5. Performance at urban locations stayed steady in the winter, with fractional  
395 error changing from 0.30 to 0.26 and fractional bias changing from +0.02 to +0.08 moving  
396 from 36 km to 1 km resolution (Fig. S3). Rural performance improved to a greater extent,  
397 with fractional error improving from 0.33 to 0.28 and fractional bias lowering from +0.21  
398 to +0.11.

399 The comparison with low-cost sensor measurements largely represents the  
400 performance of the model in terms of urban  $\text{PM}_{2.5}$  predictions. The performance metrics of



401 PMCAMx-v2.0 when compared to measurements from low-cost sensors are shown in  
402 Table 3. Moving from low to high resolution, the predictions go from no bias (-0.02) to a  
403 bias of +0.24. Due to the slight overprediction of the urban-rural gradient seen earlier  
404 (particularly with EC), the high resolution would likely lead to more positive biases when  
405 compared to a largely urban network. Fractional error increases slightly, but still exhibits  
406 good performance moving from 0.33 to 0.37.

407

## 408 **5.2 Summer**

409 In the summer period, (Fig. 6) the model performance improved as the resolution  
410 increased from 36 km to 1 km. Fractional error decreased from 0.53 to 0.48, while  
411 fractional bias increased from -0.46 to -0.39. In July, performance at the urban locations  
412 significantly increased with resolution (Fig. S4). Fractional error decreased from 52% at  
413 36 x 36 km to 0.42 at 1 x 1 km. Fractional bias also improved from -0.46 at the coarse grid  
414 resolution to -0.39 at the finest scale. Rural predictions of PM<sub>2.5</sub> were also better with  
415 increasing resolution in the summer. Fractional error decreased from 0.31 to 0.22 while  
416 fractional bias decreased from +0.05 to -0.05.

417 Larger improvements are seen with increasing resolution during the summer when  
418 compared to measurements from low-cost sensors. Starting from a large negative bias of  
419  $-5.4 \mu\text{g m}^{-3}$  (fractional bias of -0.48) at the 36 x 36 km resolution, performance consistently  
420 improved with each increasing resolution step with the bias eventually reaching  $-3.7 \mu\text{g m}^{-3}$   
421 (fractional bias of -0.27) at the 1 x 1 km. There was also a reduction in fractional error  
422 from 0.52 at the coarse to 0.41 at the fine 1 x 1 km resolution. These metrics are  
423 encouraging, although they are likely impacted by an overprediction of the urban-rural  
424 gradient, similar to winter. Improvement of the secondary PM<sub>2.5</sub> predictions is still the  
425 largest source of error between predictions and this source of measurements.

426

## 427 **6 Evaluation of Novel Emissions Surrogates**

428 For commercial cooking, the normalized restaurant count was used to distribute the  
429 emissions from the sector in space within the 1 x 1 km domain. Geographical information  
430 was collected for all restaurant locations in the inner domain from the Google Places  
431 Application Programming Interface. This includes southwestern Pennsylvania as well as



432 parts of eastern Ohio and northern West Virginia. To allocate on-road traffic emissions, the  
433 output from the traffic model of Ma et al. (2020) was used. This model simulated hourly  
434 traffic using data from the Pennsylvania Department of Transportation sites located  
435 throughout the inner modeling domain. Changes in the spatial distribution of cooking and  
436 on-road traffic emissions are illustrated in the supplementary material (Fig. S5-S8). These  
437 novel emissions surrogates resulted in larger emissions of both traffic and cooking in the  
438 downtown area. In the case of on-road traffic, major highways in the inner domain are  
439 emphasized with the new surrogates.

440 For both February and July 2017, the largest observed change when using the novel  
441 surrogates is an increase in predicted  $\text{PM}_{2.5}$  of around  $3 \mu\text{g m}^{-3}$  in the downtown Pittsburgh  
442 area (Fig. 7). Differences in predicted  $\text{PM}_{2.5}$  concentrations outside of the urban areas of  
443 the inner domain are very small (less than  $0.5 \mu\text{g m}^{-3}$  in magnitude).

444 Model performance at  $1 \times 1 \text{ km}$  resolution is detailed in Table 4. Negligible changes  
445 in performance were seen using EPA regulatory  $\text{PM}_{2.5}$  data in February 2017. Small  
446 improvements were seen at regulatory sites in July 2017, where fractional error was  
447 reduced from 51% to 48% and fractional bias increased from -43% to -39%. A positive  
448 shift in fractional bias was seen with the use of the new surrogates during both periods  
449 when compared to low-cost sensor measurements, resulting in a modest overprediction of  
450  $\text{PM}_{2.5}$  in the winter (+0.24 fractional bias) and a modest underprediction of  $\text{PM}_{2.5}$  in the  
451 summer (-0.27 fractional bias). The larger changes when compared to the low-cost sensor  
452 measurements are a result of the location of the low-cost sensors in urban areas, where the  
453 new surrogates predicted elevated  $\text{PM}_{2.5}$  mass concentrations.

## 454 **7 Conclusions**

455 We applied PMCAMx-v2.0 over southwestern Pennsylvania during February and  
456 July 2017 at grid resolutions of 36 km, 12 km, 4 km and 1 km. Emissions were calculated  
457 for the relevant grids by using the spatial surrogates provided along with the 2011 NEI for  
458 all emissions sectors except traffic and cooking, for which  $1 \times 1 \text{ km}$  spatial surrogates were  
459 developed.

460 PMCAMx predicts winter sulfate, elemental carbon and organic aerosol  
461 concentrations with fractional biases below 10% at high resolution. Nitrate concentrations  
462 are overpredicted (bias  $+1.4 \mu\text{g m}^{-3}$ ) following the trend of previous studies in both the US



463 and Europe. Agreement with total PM<sub>2.5</sub> measurements is also encouraging with a  
464 fractional bias of +5%. Variability between urban and rural predictions of local pollutants  
465 EC and organic aerosol (OA) are reproduced well in the winter period. Underpredictions  
466 of summer OA concentrations led to underpredictions of total PM<sub>2.5</sub> mass. Summer sulfate  
467 is reproduced with fractional bias of -21% and elemental carbon (EC) is predicted with  
468 fractional bias of -33%. Nitrate is similarly overpredicted in the summer with fractional  
469 bias of +70% although with a much smaller magnitude than in the winter (+0.4 μg m<sup>-3</sup>).  
470 Improvement of the treatment of dust in the model is required to better model the  
471 distribution of particulate nitrate between PM<sub>2.5</sub> and PM<sub>10</sub> modes. Differences between  
472 urban and rural EC is also predicted well in the summer, while OA is predicted to vary  
473 little between urban and rural locations. This is indicative of a greater contribution of  
474 secondary species to OA during this period. Improvements to SOA formation chemistry  
475 within the model, particularly from biogenic sources outside of the inner modeling domain,  
476 will likely have a significant impact on PM<sub>2.5</sub> predictions around the city of Pittsburgh.  
477 This, along with the improvement of dust treatment in the model, are topics of future work  
478 for model improvement.

479 PM<sub>2.5</sub> prediction performance improved in almost all cases when increasing the  
480 resolution from 36 km to 1 km. Underpredictions at urban sites and overpredictions at rural  
481 sites were reduced at the same time. This is true when comparing against measurements  
482 from regulatory sites as well as low-cost monitors. The improved performance here is  
483 evidence of the enhanced ability of the model to capture important urban-rural gradients in  
484 PM<sub>2.5</sub> pollution by increasing the resolution of predictions to 1 x 1 km.

485

486 *Code Availability.* The PMCAMx-v2.0 code is available in Zenodo at  
487 <https://doi.org/10.5281/zenodo.6772851> (Dinkelacker et al., 2022). License (for files):  
488 GNU General Public License v3.0.

489

490 *Author contributions.* BTD performed the PMCAMx simulations, analyzed the results, and  
491 wrote the manuscript. PGR wrote the code for data analysis, prepared anthropogenic  
492 emissions and other inputs for the PMCAMx simulations, and assisted in writing the  
493 manuscript. IK set up the WRF simulations and assisted in the preparation of the





494 meteorological inputs. SNP and PJA designed and coordinated the study and helped in the  
495 writing of the paper. All authors reviewed and commented on the manuscript.

496

497 *Competing Interests.* The authors declare that they have no conflict of interest.

498 *Financial support.* This work was supported by the Center for Air, Climate, and Energy  
499 Solutions (CACES) which was supported under Assistance Agreement No. R835873  
500 awarded by the U.S. Environmental Protection Agency and the Horizon-2020 Project  
501 REMEDIA of the European Union under grant agreement No 874753.

502

### 503 **References**

504 Allan, J. D.; Williams, P. I.; Morgan, W. T.; Martin, C. L.; Flynn, M. J.; Lee, J.; Nemitz,  
505 E.; Phillips, G. J.; Gallagher, M. W.; Coe, H.: Contributions from transport, solid  
506 fuel burning and cooking to primary organic aerosols in two UK cities, *Atmos.*  
507 *Chem. Phys.*, 10, 647–668. doi:10.5194/acp-10-647-2010, 2010.

508 Anand, S.: The concern for equity in health, *JECH*, 56, 485–487.  
509 doi:10.1136/jech.56.7.485, 2002.

510 Arunachalam, S., Holland, A., Do, B., Abraczkas, M.: A quantitative assessment of the  
511 influence of grid resolution on predictions of future-year air quality in North  
512 Carolina, USA, *Atmos. Environ.*, 40, 5010–5026.  
513 doi:10.1016/j.atmosenv.2006.01.024, 2006.

514 Carter, W.P.L.: Documentation of the SAPRC-99 chemical mechanism for VOC reactivity  
515 assessment., 1999.

516 Day, M.C., Pandis, S.N.: Effects of a changing climate on summertime fine particulate  
517 matter levels in the eastern U.S., *J. Geophys. Res.*, 120, 5706–5720.  
518 doi:10.1002/2014JD022889, 2015.

519 Dinkelacker, B.T., Garcia Rivera, P., Kioutsioukis, I., Adams, P., Pandis, S.N.: Source  
520 Code for PMCAMx-v2.0: "High-resolution modeling of fine particulate matter in  
521 an urban area using PMCAMx-v2.0", Zenodo [model code],  
522 <https://doi.org/10.5281/zenodo.6772851>, 2022.

523 Dockery, D.W., Pope, C.A.: Acute Respiratory Effects of Particulate Air Pollution, *Annu.*  
524 *Rev. Public Health*, 15, 107–132. doi:10.1146/annurev.pu.15.050194.000543,



- 525           1994.
- 526 Donahue, N.M., Robinson, A.L., Stanier, C.O., Pandis, S.N.: Coupled partitioning,  
527           dilution, and chemical aging of semivolatile organics, *Environ. Sci. Technol.*, 40,  
528           2635–2643. doi:10.1021/es052297c, 2006.
- 529 ENVIRON: CAMx (Comprehensive Air Quality Model with Extensions) User's Guide  
530           Version 4.20, 2006.
- 531 Eyth, A., Vukovich, J.: Technical Support Document (TSD): Preparation of emissions  
532           inventories for the version 6.2, 2011 emissions modeling platform., 2016.
- 533 Fahey, K. M.; Pandis, S. N.: Optimizing model performance: variable size resolution in  
534           cloud chemistry modeling, *Atmos. Environ.*, 35, 4471–4478, doi:10.1016/S1352-  
535           2310(01)00224-2, 2001.
- 536 Fountoukis, C., Koraj, D., Denier van der Gon, H.A.C., Charalampidis, P.E., Pilinis, C.,  
537           Pandis, S.N.: Impact of grid resolution on the predicted fine PM by a regional 3-D  
538           chemical transport model, *Atmos. Environ.*, 68, 24–32.  
539           doi:10.1016/j.atmosenv.2012.11.008, 2013.
- 540 Garcia Rivera, P., Dinkelacker, B. T., Kioutsioukis, I., Adams, P. J., and Pandis, S. N.:  
541           Source-resolved variability of fine particulate matter and human exposure in an  
542           urban area, *Atmos. Chem. Phys.*, 22, doi:10.5194/acp-22-2011-2022, 2022.
- 543 Gaydos, T.M.; Koo, B.; Pandis, S.N.; Chock, D.P.: Development and applicaiton of an  
544           efficient moving sectional approach for the solution of the atmospheric aerosol  
545           condensation/evaporation equations, *Atmos. Environ.*, 37, 3303–3316,  
546           doi:10.1016/S1352-2310(03)00267-X, 2003.
- 547 Gu, P., Li, H.Z., Ye, Q., Robinson, E.S., Apte, J.S., Robinson, A.L., Presto, A.A.: Intracity  
548           variability of particulate matter exposure is driven by carbonaceous sources and  
549           correlated with land-use variables, *Environ. Sci. Technol.*, 52, 11545–11554.  
550           doi:10.1021/acs.est.8b03833, 2018.
- 551 Karydis, V.A., Tsimpidi, A.P., Fountoukis, C., Nenes, A., Zavala, M., Lei, W., Molina,  
552           L.T., Pandis, S.N.: Simulating the fine and coarse inorganic particulate matter  
553           concentrations in a polluted megacity, *Atmos. Environ.*, 44, 608–620.  
554           doi:10.1016/j.atmosenv.2009.11.023, 2010.
- 555 Kumar, N., Russell, A.G.: Multiscale air quality modeling of the Northeastern United



- 556 States, *Atmos. Environ.*, 30, 1099–1116. doi:10.1016/1352-2310(95)00317-7,  
557 1996.
- 558 Lane, T.E., Donahue, N.M., Pandis, S.N.: Effect of NO<sub>x</sub> on secondary organic aerosol  
559 concentrations, *Environ. Sci. Technol.*, 42, 6022–6027. doi:10.1021/es703225a,  
560 2008.
- 561 Lanz, V. A.; Alfarra, M. R.; Baltensperger, U.; Buchmann, B.; Hueglin, C.; Prevot, A. S.  
562 H.: Source apportionment of submicron organic aerosols at an urban site by factor  
563 analytical modelling of aerosol mass spectra, *Atmos. Chem. Phys.*, 7, 1503-1522.  
564 doi:10.5194/acp-7-1503-2007, 2007.
- 565 Ma, W., Pi, X., Qian, S.: Estimating multi-class dynamic origin-destination demand  
566 through a forward-backward algorithm on computational graphs. *Transportation*  
567 *Research Part C: Emerging Technologies*, 119, 102747, doi:10.1016/j.trc.2020.  
568 102747, 2020.
- 569 Malings, C., Tanzer, R., Haurlyliuk, A., Saha, P.K., Robinson, A.L., Presto, A.A.,  
570 Subramanian, R.: Fine particle mass monitoring with low-cost sensors: corrections  
571 and long-term performance evaluation, *Aerosol Sci. Tech.*, 54, 160-174, doi:  
572 10.1080/02786826.2019.1623863, 2019.
- 573 Murphy, B.N., Pandis, S.N.: Exploring summertime organic aerosol formation in the  
574 eastern United States using a regional-scale budget approach and ambient  
575 measurements, *J. Geophys. Res.*, 115, D24 doi:10.1029/2010JD014418, 2010.
- 576 Nenes, A., Pandis, S.N., Pilinis, C.: ISORROPIA: a new thermodynamic equilibrium  
577 model for multiphase multicomponent inorganic aerosols, *Aquat. Geochem.*, 4,  
578 123–152, doi:10.1023/A:1009604003981, 1998.
- 579 Pan, S., Choi, Y., Roy, A., Jeon, W.: Allocating emissions to 4 km and 1 km horizontal  
580 spatial resolutions and its impact on simulated NO<sub>x</sub> and O<sub>3</sub> in Houston, TX. *Atmos.*  
581 *Environ.*, 164, 398–415, 2017.
- 582 Robinson, E.S., Gu, P., Ye, Q., Li, H.Z., Shah, R.U., Apte, J.S., Robinson, A.L., Presto,  
583 A.A.: Restaurant Impacts on Outdoor Air Quality: Elevated Organic Aerosol Mass  
584 from Restaurant Cooking with Neighborhood-Scale Plume Extents, *Environ. Sci.*  
585 *Technol.*, 52, 9285–9294, doi:10.1021/acs.est.8b02654, 2018.
- 586 Skyllakou, K., Garcia Rivera, P., Dinkelacker, B., Karnezi, E., Kioutsioukis, I., Hernandez,



587 C., Adams, P. J., Pandis, S. N.: Changes in PM<sub>2.5</sub> concentrations and their sources  
588 in the US from 1990 to 2010, *Atmos. Chem. Phys.*, 21, 17115-17132,  
589 doi:10.5194/acp-21-17115-2021, 2021.

590 Stroud, C.A., Makar, P.A., Moran, M.D., Gong, W., Gong, S., Zhang, J., Hayden, K.,  
591 Mihele, C., Brook, J.R., Abbatt, J.P.D., Slowik, J.G.: Impact of model grid spacing  
592 on regional- and urban- scale air quality predictions of organic aerosol, *Atmos.*  
593 *Chem. Phys.*, 11, 3107–3118, doi:10.5194/acp-11-3107-2011, 2011.

594 Tsimpidi, A.P., Karydis, V.A., Zavala, M., Lei, W., Molina, L.T., Ulbrich, I.M., Jimenez,  
595 J.L., Pandis, S.N.: Evaluation of the volatility basis-set approach for the simulation  
596 of organic aerosol formation in the Mexico City metropolitan area, *Atmos. Chem.*  
597 *Phys. Disc.*, 9, 13693–13737, doi:10.5194/acpd-9-13693-2009, 2010.

598 U.S. EPA: User guide: Air Quality System, Report, Research Triangle Park, N.C., available  
599 at: <http://www.epa.gov/ttn/airs/airsaqs/manuals/AQSUserGuide.pdf> (last access:  
600 January 2022), 2002.

601 Zakoura, M., Pandis, S.N.: Improving fine aerosol nitrate predictions using a Plume-in-  
602 Grid modeling approach, *Atmos. Environ.*, 215, 116887. doi:10.1016/  
603 j.atmosenv.2019.116887, 2019.

604 Zakoura, M., Pandis, S.N.: Overprediction of aerosol nitrate by chemical transport models:  
605 The role of grid resolution, *Atmos. Environ.*, 187, 390–400, doi:10.1016/  
606 j.atmosenv.2018.05.066, 2018.

607 Zimmerman, N., Presto, A.A., Kumar, S.P.N., Gu, J., Hauryliuk, A., Robinson, E.S.,  
608 Robinson, A.L., Subramanian, R.: A machine learning calibration model using  
609 random forests to improve sensor performance for lower-cost air quality  
610 monitoring, *Atmos. Meas. Tech.*, 11, 291–313, doi:10.5194/amt-11-291-2018,  
611 2018.

612  
613



614 **Table 1.** Comparison of daily average high-resolution PMCAMx-v2.0 predictions with  
 615 daily EPA-CSN measurements during February and July 2017.  
 616

<b>February 2017</b>						
	<b>Sulfate</b>	<b>Nitrate</b>	<b>Ammon.</b>	<b>Elemental Carbon</b>	<b>Organic Aerosol</b>	<b>PM<sub>2.5</sub><sup>a</sup></b>
Measured Avg. ( $\mu\text{g m}^{-3}$ )	1.92	1.51	0.91	1.08	4.37	10.34
Predicted Avg. ( $\mu\text{g m}^{-3}$ )	1.70	2.90	1.62	0.94	3.68	10.52
Error ( $\mu\text{g m}^{-3}$ )	0.79	1.54	1.03	0.78	2.15	3.02
Fractional Error	0.41	0.83	0.96	0.71	0.53	0.30
Bias ( $\mu\text{g m}^{-3}$ )	-0.22	1.40	0.71	-0.14	-0.68	0.18
Fractional Bias	-0.02	0.81	0.83	-0.08	-0.01	0.05

<b>July 2017</b>						
	<b>Sulfate</b>	<b>Nitrate</b>	<b>Ammon.</b>	<b>Elemental Carbon</b>	<b>Organic Aerosol</b>	<b>PM<sub>2.5</sub><sup>a</sup></b>
Measured Avg. ( $\mu\text{g m}^{-3}$ )	2.04	0.26	0.53	0.74	4.46	11.24
Predicted Avg. ( $\mu\text{g m}^{-3}$ )	1.60	0.68	0.79	0.56	2.67	7.26
Error ( $\mu\text{g m}^{-3}$ )	1.12	0.45	0.39	0.39	2.46	4.67
Fractional Error	0.62	0.82	0.62	0.60	0.67	0.49
Bias ( $\mu\text{g m}^{-3}$ )	-0.44	0.42	0.26	-0.18	-1.85	-4.01
Fractional Bias	-0.21	0.70	0.44	-0.33	-0.47	-0.39

618 <sup>a</sup> Measurements from the regulatory EPA monitors.  
 619



620 **Table 2.** Comparison of daily average PMCAMx-v2.0 predicted PM<sub>2.5</sub> concentrations  
 621 during February and July 2017 with daily measurements from 17 EPA regulatory  
 622 monitors.  
 623

	36 x 36 km	12 x 12 km	4 x 4 km	1 x 1 km
<b>February 2017</b>				
Measured Avg. ( $\mu\text{g m}^{-3}$ )	10.34	10.34	10.34	10.34
Predicted Avg. ( $\mu\text{g m}^{-3}$ )	9.78	9.68	10.49	10.52
Error ( $\mu\text{g m}^{-3}$ )	3.35	3.16	3.04	3.02
Fractional Error	0.34	0.32	0.30	0.30
Bias ( $\mu\text{g m}^{-3}$ )	-0.56	-0.66	0.15	0.18
Fractional Bias	-0.09	-0.10	0.06	0.05
<b>July 2017</b>				
Measured Avg. ( $\mu\text{g m}^{-3}$ )	11.24	11.24	11.24	11.24
Predicted Avg. ( $\mu\text{g m}^{-3}$ )	6.90	6.86	7.26	7.23
Error ( $\mu\text{g m}^{-3}$ )	4.89	5.05	4.67	4.65
Fractional Error	0.53	0.53	0.49	0.48
Bias ( $\mu\text{g m}^{-3}$ )	-4.34	-4.39	-3.98	-4.01
Fractional Bias	-0.45	-0.47	-0.39	-0.39

624



625 **Table 3.** Comparison of daily average PMCAMx-v2.0 predicted PM<sub>2.5</sub> concentrations  
 626 during February and July 2017 with daily low-cost sensor (RAMP) measurements.  
 627

	36 x 36 km	12 x 12 km	4 x 4 km	1 x 1 km
<b>February 2017</b>				
Measured Avg. ( $\mu\text{g m}^{-3}$ )	11.65	11.65	11.65	11.65
Predicted Avg. ( $\mu\text{g m}^{-3}$ )	10.23	11.64	12.04	13.50
Error ( $\mu\text{g m}^{-3}$ )	4.53	4.53	4.51	5.12
Fractional Error	0.33	0.33	0.34	0.37
Bias ( $\mu\text{g m}^{-3}$ )	-1.43	-0.02	0.4	1.85
Fractional Bias	-0.02	<0.01	0.14	0.24
<b>July 2017</b>				
Measured Avg. ( $\mu\text{g m}^{-3}$ )	12.59	12.59	12.59	12.59
Predicted Avg. ( $\mu\text{g m}^{-3}$ )	7.19	7.44	8.06	8.83
Error ( $\mu\text{g m}^{-3}$ )	5.60	5.70	5.29	4.89
Fractional Error	0.51	0.51	0.46	0.42
Bias ( $\mu\text{g m}^{-3}$ )	-5.40	-5.15	-4.53	-3.76
Fractional Bias	-0.48	-0.43	-0.36	-0.27

628  
 629



630 **Table 4.** Performance of daily average predicted total PM<sub>2.5</sub> concentrations compared to  
 631 daily measurements from regulatory sites and low-cost sensors with the use of old  
 632 surrogates and new surrogates for on-road traffic and commercial cooking.  
 633

<b>February 2017</b>				
	<b>Old Surrogates</b>		<b>New Surrogates</b>	
	Regulatory network	Low-cost sensors	Regulatory network	Low-cost sensors
<b>Observed Average</b> ( $\mu\text{g m}^{-3}$ )	10.34	11.65	10.34	11.65
<b>Predicted Average</b> ( $\mu\text{g m}^{-3}$ )	10.23	11.32	10.52	13.50
<b>Error</b> ( $\mu\text{g m}^{-3}$ )	2.94	4.12	3.02	5.12
<b>Fractional Error</b>	0.29	0.31	0.30	0.37
<b>Bias</b> ( $\mu\text{g m}^{-3}$ )	-0.11	-0.33	0.18	1.85
<b>Fractional Bias</b>	-0.04	0.08	0.05	0.24

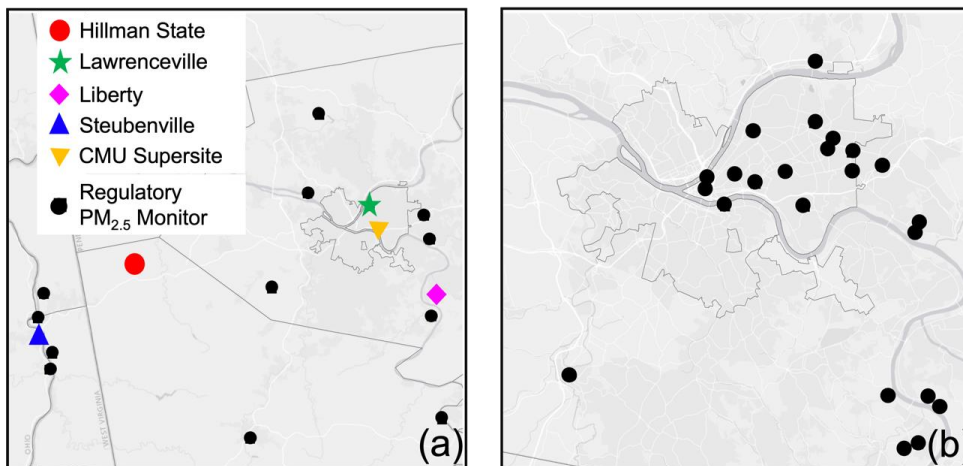
<b>July 2017</b>				
	<b>Old Surrogates</b>		<b>New Surrogates</b>	
	Regulatory network	Low-cost sensors	Regulatory network	Low-cost sensors
<b>Observed Average</b> ( $\mu\text{g m}^{-3}$ )	11.24	12.58	11.24	12.58
<b>Predicted Average</b> ( $\mu\text{g m}^{-3}$ )	7.09	7.98	7.26	8.83
<b>Error</b> ( $\mu\text{g m}^{-3}$ )	4.91	5.32	4.67	4.89
<b>Fractional Error</b>	0.51	0.47	0.49	0.42
<b>Bias</b> ( $\mu\text{g m}^{-3}$ )	-4.33	-4.61	-4.01	-3.76
<b>Fractional Bias</b>	-0.43	-0.37	-0.39	-0.27

634  
 635





636



637

638

639

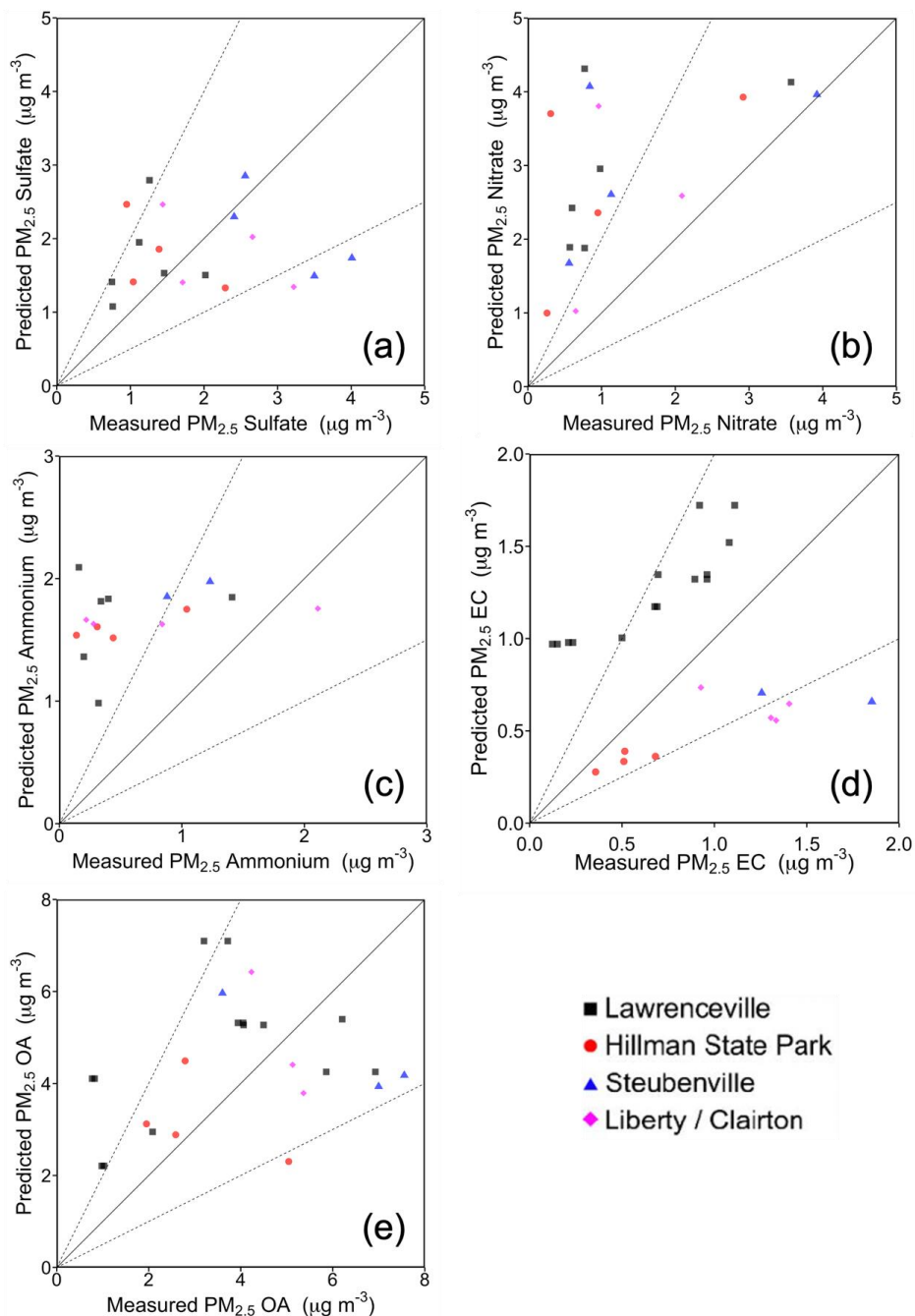
640

**Figure 1.** Monitoring sites. (a) Particulate matter speciation measurement sites from EPA-CSN and PM<sub>2.5</sub> regulatory monitors. (b) low-cost sensor sites.

641

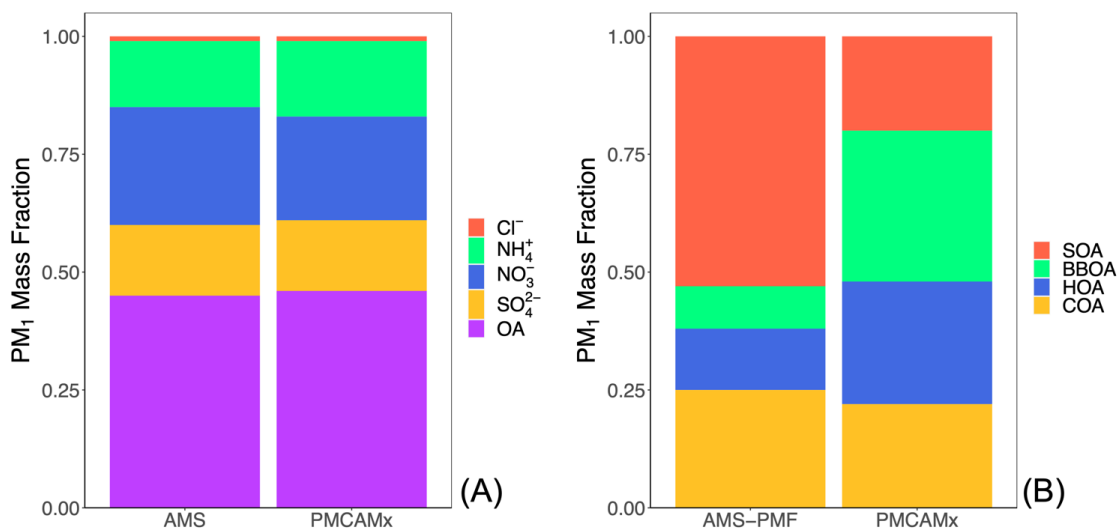


642



643  
644  
645  
646

**Figure 2.** Comparison of daily average PMCAMx-v2.0 predicted concentrations of PM<sub>2.5</sub> (a) sulfate, (b) nitrate, (c) ammonium, (d) elemental carbon, and (e) organic aerosol with daily measurements from EPA-CSN sites during February 2017.

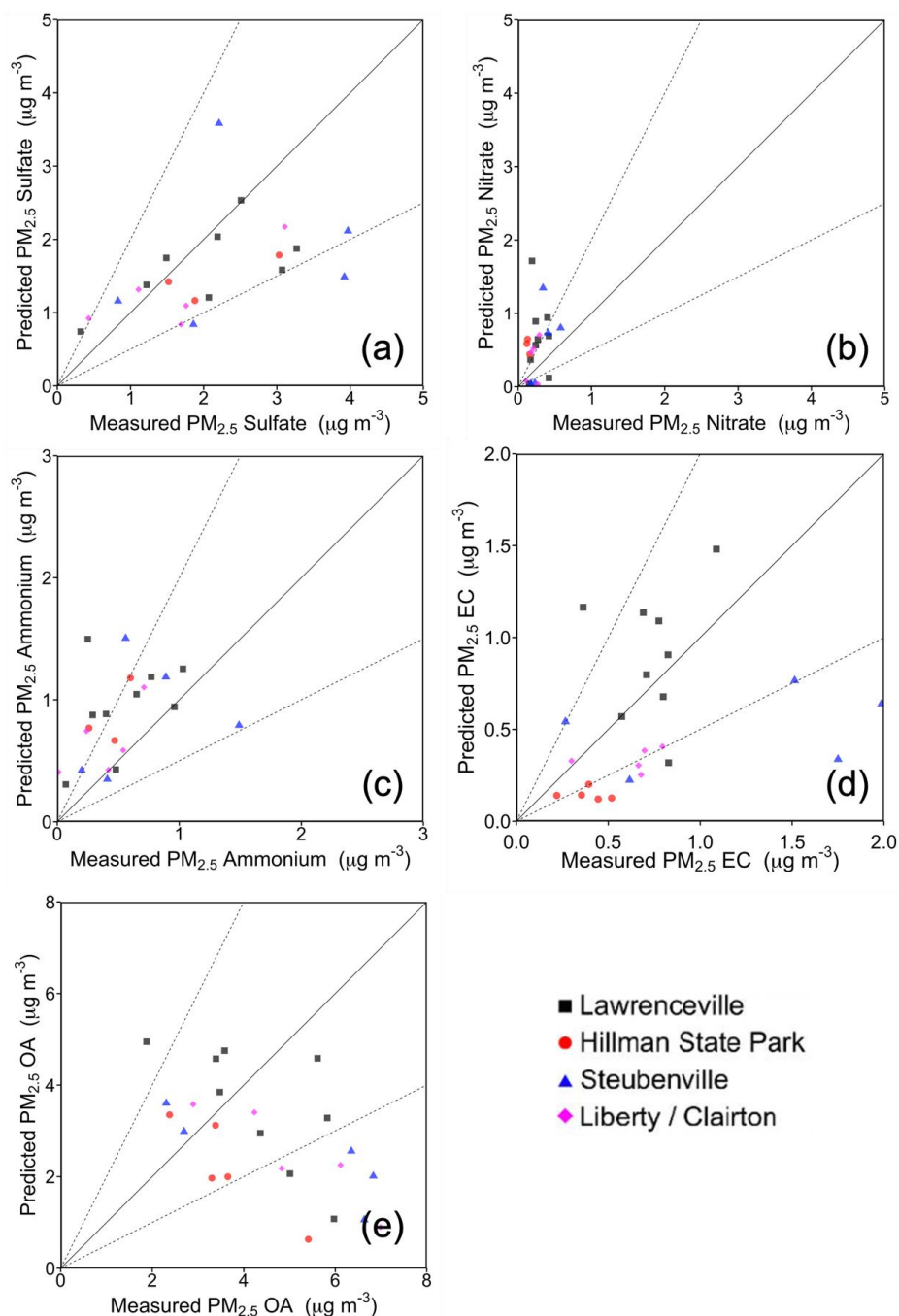


647

648

649 **Figure 3.** (a) Comparison of PMCAMx-v2.0 predicted composition of PM<sub>1</sub> with the  
650 corresponding AMS measurements at the CMU site and (b) organic aerosol composition  
651 based on the PMF analysis of the AMS measurements and predicted composition.

652

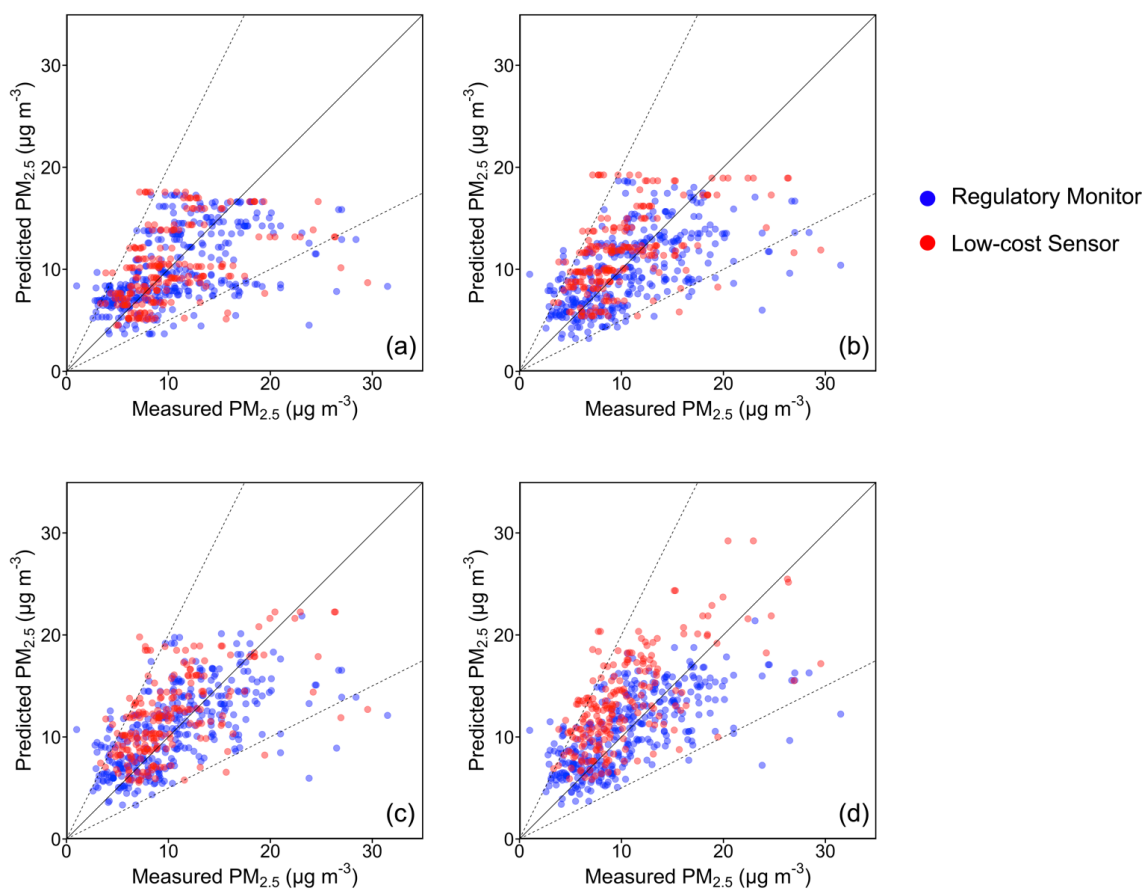


653  
654  
655  
656

**Figure 4.** Comparison of PMCAMx-v2.0 predicted concentrations of PM<sub>2.5</sub> (a) sulfate, (b) nitrate, (c) ammonium, (d) elemental carbon, and (e) organic aerosol with measurements from EPA-CSN sites during July 2017.



657



658

659

660

661

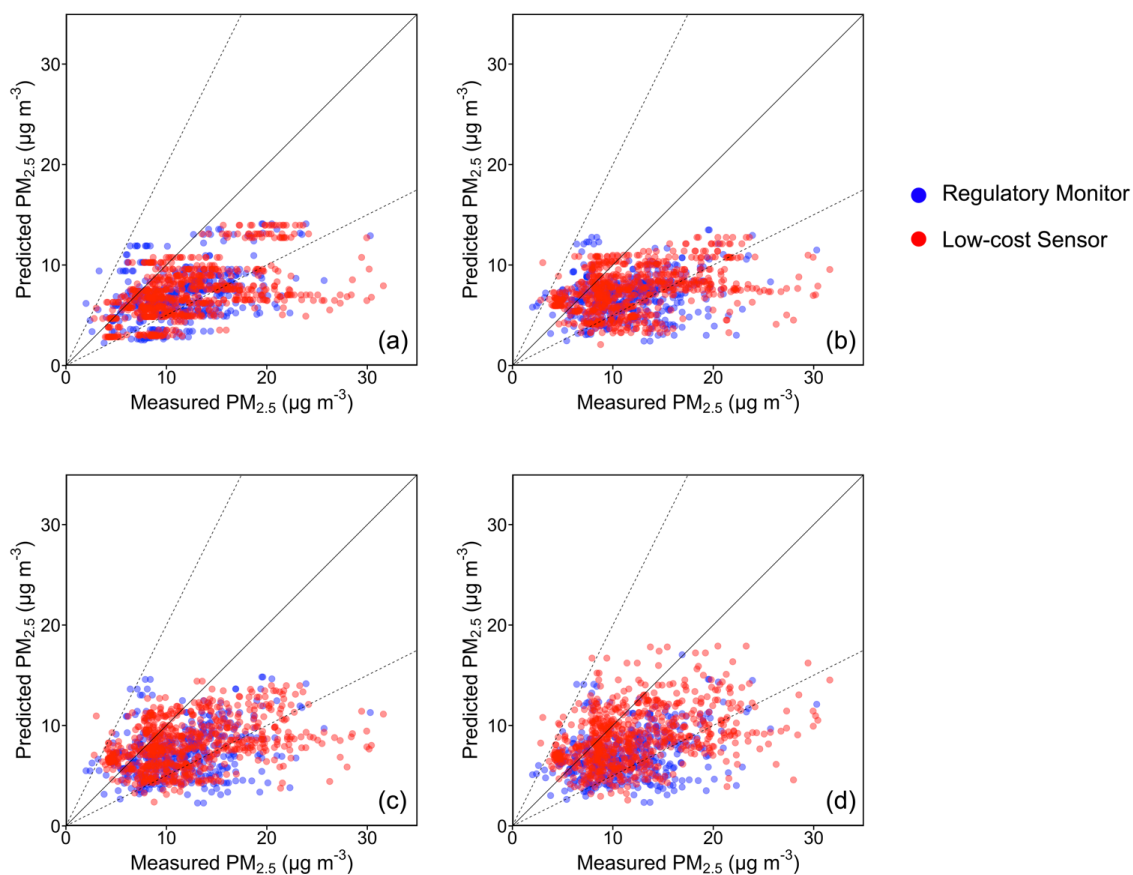
662

**Figure 5.** Comparison of daily average PMCAMx-v2.0 predicted concentrations of  $PM_{2.5}$  with daily regulatory measurements and daily low-cost sensor measurements at (a) 36 x 36, (b) 12 x 12, (c) 4 x 4, and (d) 1 x 1 km during February 2017.

663



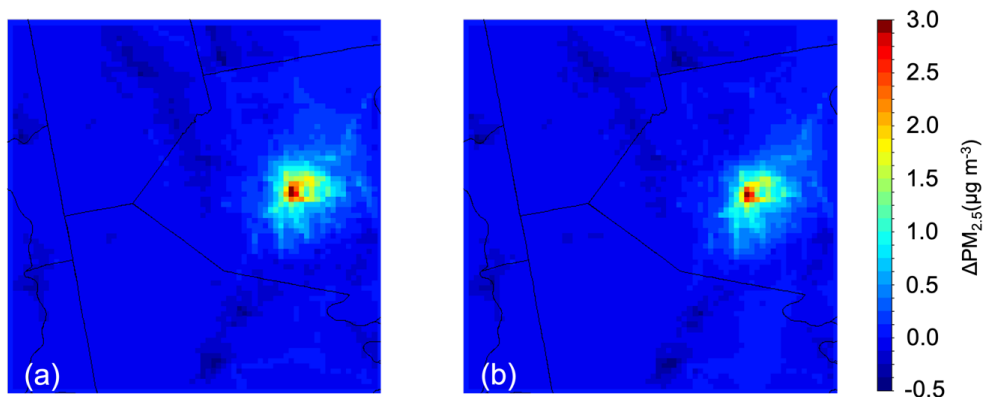
664



665  
666

667 **Figure 6.** Comparison of daily average PMCAMx-v2.0 predicted concentrations of  $PM_{2.5}$   
668 with daily regulatory measurements and daily low-cost sensor measurements at (a) 36 x  
669 36, (b) 12 x 12, (c) 4 x 4, and (d) 1 x 1 km during July 2017.

670



671  
672  
673  
674  
675  
676

**Figure 7.** Difference between predicted monthly average  $PM_{2.5}$  mass concentration when using novel surrogates and original surrogates in (a) February 2017 and (b) July 2017 for the 1 x 1 km resolution simulation grid. A positive value indicates a higher concentration predicted with the novel surrogates.